Environmental Research 224 (2023) 115550

Contents lists available at ScienceDirect

Environmental Research

journal homepage: www.elsevier.com/locate/envres

Catalytic co-pyrolysis of oil palm trunk and polypropylene with Ni–Mo/TiO_2 and Ni/Al_2O_3: Oil composition and mechanism

Liza Melia Terry [a], Melvin Xin Jie Wee [b], Jiuan Jing Chew [a], Deni Shidqi Khaerudini [c], Nono Darsono [c], Aqsha Aqsha [d], Agus Saptoro [b], Jaka Sunarso [a,*]

[a] Research Centre for Sustainable Technologies, Faculty of Engineering, Computing and Science, Swinburne University of Technology, Jalan Simpang Tiga, 93350, Kuching, Sarawak, Malaysia
[b] Department of Chemical and Energy Engineering, Curtin University Malaysia, CDT 250, Miri, Sarawak, 98009, Malaysia
[c] Research Center for Advanced Materials, National Research and Innovation Agency (BRIN), Bld. 440 Kawasan Puspiptek Serpong, South Tangerang, 15314, Banten, Indonesia
[d] Department of Bioenergy Engineering and Chemurgy, Faculty of Industrial Technology, Institut Teknologi Bandung, Bandung, 40132, Jawa Barat, Indonesia

ARTICLE INFO

Handling Editor: Aijie Wang

Keywords:
Catalyst
Nickel-based
Nickel-molybdenum based
Oil palm biomass
Pyrolysis oil

ABSTRACT

Pyrolysis oil from oil palm biomass can be a sustainable alternative to fossil fuels and the precursor for synthesizing petrochemical products due to its carbon-neutral properties and low sulfur and nitrogen content. This work investigated the effect of applying mesoporous acidic catalysts, Ni–Mo/TiO_2 and Ni/Al_2O_3, in a catalytic co-pyrolysis of oil palm trunk (OPT) and polypropylene (PP) from 500 to 700 °C. The obtained oil yields varied between 12.67 and 19.50 wt.% and 12.33–17.17 wt.% for Ni–Mo/TiO_2 and Ni/Al_2O_3, respectively. The hydrocarbon content in oil significantly increased up to 54.07–58.18% and 37.28–68.77% after adding Ni–Mo/TiO_2 and Ni/Al_2O_3, respectively. The phenolic compounds content was substantially reduced to 8.46–20.16% for Ni–Mo/TiO_2 and 2.93–14.56% for Ni/Al_2O_3. Minor reduction in oxygenated compounds was noticed from catalytic co-pyrolysis, though the parametric effects of temperature and catalyst type remain unclear. The enhanced deoxygenation and cracking of phenolic and oxygenated compounds and the PP decomposition resulted in increased hydrocarbon production in oil during catalytic co-pyrolysis. Catalyst addition also promoted the isomerization and oligomerization reactions, enhancing the formation of cyclic relative to aliphatic hydrocarbon.

1. Introduction

Fossil fuels are essential building blocks in the petrochemical industries for producing materials such as plastics, synthetic fibres, rubbers, lubricants, detergents, and solvents (Keim, 2010; Speight, 2011). However, their non-renewable nature poses a sustainability risk, prompting the search for sustainable alternatives based on renewable biomass sources (Ozturk et al., 2017). Oil produced from pyrolysis of lignocellulosic biomass, such as oil palm biomass, can be a sustainable alternative to fossil fuels, given its carbon-neutral properties with low sulfur and nitrogen content (Martínez et al., 2014; Palamanit et al., 2019). During pyrolysis, the thermal decomposition of oil palm biomass may produce more than 300 chemical compounds in the oil, which can be used as precursors for synthesizing petrochemical products (Keim, 2010; Machado et al., 2022). Oil palm biomass-derived pyrolysis oil mainly consists of oxygenated compounds due to its high oxygen content in raw biomass. Such oil requires modification to improve the hydrocarbon content (Palamanit et al., 2019). Co-pyrolysis of oil palm biomass with plastics like polypropylene (PP) is a promising method for increasing hydrocarbon content (Al-Maari et al., 2021). PP, rich in carbon and hydrogen, provides the hydrocarbon pool required for the deoxygenation reaction of oxygenated compounds from biomass to form hydrocarbons such as aliphatic and aromatic hydrocarbons in oil.

Solid acidic catalysts can further promote the deoxygenation reactions (i.e., dehydration, decarbonylation, and decarboxylation) of pyrolytic volatiles to improve the hydrocarbon content in pyrolysis oil (Hassan et al., 2019; Shafaghat et al., 2019; Zhang et al., 2016). Due to its excellent catalytic performance for deoxygenation, which generates hydrocarbons such as olefins, aliphatic, and aromatic hydrocarbons, high-acidity zeolites have been widely used in several studies

* Corresponding author. Research Centre for Sustainable Technologies, Faculty of Engineering, Computing and Science, Swinburne University of Technology, Jalan Simpang Tiga, 93350, Kuching, Sarawak, Malaysia.
E-mail addresses: jsunarso@swinburne.edu.my, barryjakasunarso@yahoo.com (J. Sunarso).

https://doi.org/10.1016/j.envres.2023.115550
Received 27 August 2022; Received in revised form 17 February 2023; Accepted 21 February 2023
Available online 24 February 2023

(Balasundram et al., 2018; Wang et al., 2020). In such a reaction, oxygen is typically removed by releasing by-products such as water, carbon dioxide, and carbon monoxide (Hassan et al., 2019). Zeolites, nonetheless, are microporous catalysts. Thus, micropore-related flow restriction can affect their deoxygenation catalytic performance, especially if relatively large molecules such as lignin-derived compounds are involved (Shafaghat et al., 2019). Such flow restriction can also cause coke formation, create pore blockage, catalyst deactivation, and catalyst poisoning, thereby reducing the performance of catalysts (Hassan et al., 2019; Shafaghat et al., 2019). To address this, mesoporous acidic catalysts such as titania (TiO_2) and alumina (Al_2O_3) based catalysts with larger pore sizes were introduced, allowing large molecules to diffuse and reducing pore blockage and catalyst deactivation (Lu et al., 2010; Zhou et al., 2019). The high chemical and thermal stabilities of TiO_2 and/or Al_2O_3-based catalysts have also sparked interest (Bagheri et al., 2014; Paranjpe, 2017). It has been proposed that doping of metals such as nickel, copper, molybdenum, cobalt, palladium, and cerium into TiO_2 and/or Al_2O_3-based catalysts can improve deoxygenation (Bagheri et al., 2014; Lu et al., 2010; Zhou et al., 2019).

Several works have evaluated TiO_2 and/or Al_2O_3-based catalysts in oil upgrading through catalytic pyrolysis and co-pyrolysis in a nitrogen atmosphere. Dong et al. (2019) compared the catalytic performances of titania-based catalysts doped with different metals, including copper (10% Cu/TiO_2), iron (10% Fe/TiO_2), and molybdenum (10% Mo/TiO_2) on the phenol conversion during the catalytic pyrolysis of corn straw lignin at 450 °C. They reported that the highest total phenol conversion was attained using 10% Mo/TiO_2, followed by 10% Cu/TiO_2, TiO_2, and then 10% Fe/TiO_2. Lu et al. (2010) studied the catalytic upgrading of oil from pyrolysis of poplar wood using the titania, zirconia, and titania-zirconia-based catalysts doped with cerium, ruthenium, and palladium at 600 °C. In general, all the catalysts reduced the sugars (i.e., levoglucosan) in the oil, while titania-zirconia-based catalysts yielded a high amount of hydrocarbons and ketones. TiO_2-based catalysts promoted the formation of phenols. Mysore Prabhakara et al. (2021) investigated the catalytic performance of γ-Al_2O_3, dolomite, and hydrotalcite (HTC) MG70 with the addition of 20 wt.% Na_2CO_3 into the catalysts during the catalytic pyrolysis of beechwood at 500 °C. All these catalysts significantly reduced the oxygenated compounds and enhanced the formation of aliphatic, monoaromatic, and polyaromatic hydrocarbons. Zhou et al. (2019) investigated the utilization of NiO/-γ-Al_2O_3 catalyst on the dehydration reaction mechanism during the pyrolysis of rice husks. Weak acid sites on Al_2O_3 were discovered to facilitate the dehydration reaction the most throughout the process. In addition, Imran et al. (2014) reported that the alumina-supported sodium carbonate (Na_2CO_3/γ-Al_2O_3) catalyst improved the quality of oil from the pyrolysis of wood fibers.

No studies have used titania and alumina-based catalysts in the co-pyrolysis of OPT and PP to improve the targeted oil composition. The mesopores in these catalysts may facilitate the diffusion rate of large molecules (i.e., compounds derived from the thermal degradation of OPT and PP) through the pores of the catalysts and promote the conversion into hydrocarbons during catalytic co-pyrolysis. This study investigated the catalytic performance of a titania-based catalyst doped with nickel-molybdenum (Ni–Mo/TiO_2) and an alumina-based catalyst with nickel (Ni/Al_2O_3) for the upgrade of oil generated from co-pyrolysis of OPT and PP. The effect of the catalysts on the oil composition was evaluated.

2. Materials and methods

2.1. Materials

OPT was collected from an oil palm plantation in Saratok, Sarawak. OPT was pre-dried in the oven at 105 °C for 24 h, ground (Fritsch rotary mill, PULVERISETTE 14), and sieved (Fritsch sieve shaker, ANALYSETTE 3 PRO) to obtain the samples with a particle size of 500 μm and below. Locally sourced PP food containers were cut into smaller sizes and sieved using a sieve shaker (Fritsch, ANALYSETTE 3 PRO) to obtain samples with a particle size of 500 μm and below. The sieved PP was stored under ambient conditions before use. Two catalysts used in this study, Ni–Mo/TiO_2 and Ni/Al_2O_3, were synthesized based on the impregnation method reported by Aqsha et al. (2015).

2.2. Nitrogen adsorption-desorption isotherm

The catalysts' specific surface area, average pore diameter, and pore volume were determined *via* nitrogen adsorption-desorption isotherm analysis (Brunauer–Emmett–Teller (BET) surface area and pore size analyzer, Quantachrome Nova 4200e). Before the analysis, the samples were degassed at 200 °C for 12 h to remove any surface-adsorbed residual moisture.

2.3. Powder X-ray diffraction (XRD)

The crystallinity of the catalysts was investigated using powder X-ray diffraction (XRD) (X-ray Diffractometer, Rigaku SmartLab). Cu-Kα radiation ($\lambda = 0.154$ nm) was used to measure the diffraction patterns in the range of 2θ from 5 to 100°.

2.4. X-ray fluorescence (XRF)

XRF was used to analyze the composition of the catalysts with an accelerating voltage of 15 kV and a current of 30 μA (Bruker S2 PUMA).

2.5. Temperature-programmed desorption with ammonia (NH_3-TPD)

The acidity of the catalysts was determined through NH_3-temperature programmed desorption (TPD) analysis (Micromeritics Chemisorb 2750). The sample was pre-treated by heating it from room temperature to 200 °C in helium gas flow for 120 min. Adsorption of NH_3 was carried out at 100 °C for 60 min (5% in He, v/v), followed by helium purging at the same temperature for another 60 min. Following that, NH_3 desorption was carried out by heating from 50 to 800 °C at a ramping rate of 10 °C min^{-1} and holding at the final temperature of 800 °C for 15 min.

2.6. Experimental runs

The catalytic co-pyrolysis was carried out in a horizontal tube furnace (MTI, GSL-1100X) with a 400 mL min^{-1} nitrogen flow rate to form an inert condition in the tube furnace. 3 g of OPT and PP mixture sample (weight ratio of OPT: PP of 1:1) with 0.3 g of catalyst were loaded into the reactor and nitrogen purged for 5 min. The reactor was heated to the desired operating temperature (i.e., 500, 600, and 700 °C) at a heating rate of 10 °C min^{-1}, with a holding time of 40 min. Afterwards, the reactor was cooled down to 200 °C while continuously purged with nitrogen gas. A cold trap in an ice bath (2–3 °C) was connected to the tube reactor outlet to collect the liquid product (oil) from the experiment. The collected oil was stored at 2–7 °C until further analysis. The non-condensable gases were released into the environment. The product yield obtained from the experiments was calculated using **Equations (1)–(3)**.

$$\text{Pyrolysis oil yield (wt.\%)} = \frac{\text{Mass of pyrolysis oil obtained (g)}}{\text{Mass of sample (g)}} \text{ x } 100\% \quad (1)$$

$$\text{Solid yield}^{*} \text{ (wt.\%)} = \frac{\text{Mass of solid obtained (g)}}{\text{Mass of sample (g)}} \text{ x } 100\% \quad (2)$$

*Solid yield refers to all solid residues collected from the experiments, including feedstock residue, catalysts, and coke.

$$\text{Gas yield (wt.\%)} = 100 \text{ wt.\%} - \text{pyrolysis oil yield (wt.\%)} - \text{solid yield (wt.\%)} \quad (3)$$

2.7. Gas chromatography-mass spectrometry (GC-MS) analysis

The composition of pyrolysis oil was determined using a gas chromatography-mass spectrometer (GC-MS) with an HP-5MS column (Agilent, 30 m length x 0.25 mm inner diameter x 0.25 m film thickness) (Agilent, 6890 N). The column oven was programmed to operate at 40 °C for 3 min. Afterwards, it was heated from 40 to 200 °C at the rate of 8 °C min^{-1} with a holding time of 10 min. The temperature was then ramped from 200 to 220 °C at a rate of 10 °C min^{-1} and held for 10 min. The column was kept at a pressure of 7.04 psi and a flow rate of 1 mL min^{-1} of helium. The split ratio of 50:1 was used in the analysis. Before the analysis, 0.2 g of pyrolysis oil was diluted in 10 mL of acetone. A syringe filter was used to filter the diluted oil sample before it was transferred to the GC sample vial and injected into the equipment *via* auto-injection mode for analysis. Compounds were identified by comparing the NIST08 mass spectral data library entries.

3. Results and discussion

3.1. Catalysts characterization

Table 1 presents the textural properties (i.e., specific surface area, pore volume, and average pore diameter) of Ni–Mo/TiO_2 and Ni/Al_2O_3. The lower specific surface area of Ni–Mo/TiO_2 compared to Ni/Al_2O_3 could be attributed to the accumulation of two types of metal particles on the catalyst's surface or within its pores (Kumar et al., 2019). Both catalysts are categorized as mesoporous since their average pore diameter sizes are between 2 and 50 nm (Thommes et al., 2015). The large pores allow large molecules, such as lignin-derived compounds, to flow in and out of the catalysts' pores for higher conversion of the compounds during the catalytic co-pyrolysis (Lu et al., 2010).

Fig. 1 depicts the acidities of the catalysts analyzed with NH_3-TPD, which reveals the acid site distribution. The temperature region where the ammonia desorption peak has located indicates the types of acid sites (i.e., weak, medium, and strong acid sites) on the surface of both catalysts. The weak acid sites correspond to the ammonia desorption peak at temperatures less than 250 °C. In comparison, the medium acid sites appear in the temperature region between 250 and 500 °C. The ammonia desorption peak, which appears at temperatures above 500 °C, represents strong acid sites (Phan et al., 2020). Strong acid sites with higher acid strength likely provide higher catalytic cracking activity for converting the compounds into desirable products through the catalyst (Li et al., 2020). Fig. 1(a) shows that most ammonia desorption peaks are between 250 and 500 °C, indicating the presence of medium acid sites for Ni–Mo/TiO_2. On the other hand, weak, medium, and strong acid sites are present on Ni/Al_2O_3 catalyst surface as the ammonia desorption peaks are detected in all three temperature regions (Fig. 1(b)). A higher peak intensity value in Ni–Mo/TiO_2 relative to that in Ni/Al_2O_3 contributes to the higher acidity in the former catalyst (Table 1).

Fig. 2 shows the powder XRD patterns of Ni–Mo/TiO_2 (upper) and Ni/Al_2O_3 (bottom) catalysts, respectively. Numerous peaks appear on the pattern of Ni–Mo/TiO_2, indicating the presence of a mix of phases. Indexing reveals three major oxide phases, i.e., anatase (TiO_2), molybdenum oxide (Mo_9O_{26}), and nickel oxide (NiO_2). An intense peak at 2θ of 25.3° is detected for TiO_2 phase, along with weak peaks at 2θ of 37.8°, 48.0°, 53.9°, 55.1°, and 62.7° (COD#96-720-6076). For Mo_9O_{26} phase, intense peaks are observed at 2θ of 24.9° and 25.3°, while weak peaks are present at 2θ of 27.3°, 32.2°, and 33.0° (ICSD#98-002-7510). NiO_2 has a weak characteristic peak at 2θ of 37.1° (ICSD#98-007-8698). Ni/Al_2O_3 has two-phase components, i.e., nickel oxide (NiO) and alumina (Al_2O_3). The intense peaks of NiO are observed at 2θ of 37.2° and 43.3° while the weak peak is detected at 2θ of 62.93° (ICDD#03-065-6920). On the other hand, the characteristic peaks of Al_2O_3 are observed at 2θ of 46.0° and 66.8° (ICDD#00-004-0858). The catalyst's composition from XRF analyses is presented in Table S1 in **Supplementary Information**.

Table 1
Textural properties and acidity of the catalysts.

Catalysts	Pore volume (cm^3 g^{-1})[a]	Average pore diameter (nm)[a]	Specific surface area (m^2 g^{-1})[b]	Acidity (mmol NH_3 g^{-1})[c]
Ni–Mo/TiO_2	0.09	11.06	32.99	2.17
Ni/Al_2O_3	0.22	8.00	109.38	0.85

Note: [a]Barrett-Joyner-Halenda (BJH) analysis; [b]Brunauer-Emmett-Teller (BET) analysis; [c]NH_3-TPD.

3.2. Product yield analysis

Fig. 3 depicts the product yield obtained from non-catalytic and catalytic co-pyrolysis of OPT and PP with Ni–Mo/TiO_2 and Ni/Al_2O_3 at temperatures ranging from 500 to 700 °C. The solid yield in Fig. 3 refers to all solid residues collected from the experiments, including feedstock residue, catalysts, and coke. When the temperature rises from 500 to 700 °C, the solid yield decreases for non-catalytic and catalytic conditions due to the decomposition of char present in the solid fraction into the oil and gas with the rising temperature. According to Zhou et al. (2013), char formation is more favorable at a lower temperature (450 °C) due to the lower decomposition rate of the feedstocks. At temperatures above 450 °C, the decomposition of feedstocks into condensable volatiles and non-condensable gases improves while char formation decreases. The pyrolysis oil yield in non-catalytic co-pyrolysis is maintained at 16 wt.% from 500 to 600 °C and drops to 11.50 wt.% when the temperature rises to 700 °C. The pyrolysis oil yield in catalytic co-pyrolysis with Ni–Mo/TiO_2 increases from 12.67 to 19.50 wt.% with the rise in temperature from 500 to 600 °C. Further increase of temperature to 700 °C reduces the oil yield to 17 wt.% due to the enhancement of the secondary reactions of the primary volatiles into the gaseous products at higher temperatures (>600 °C) (Fan et al., 2017; Zhou et al., 2013). The highest pyrolysis oil yield obtained from catalytic co-pyrolysis of Ni/Al_2O_3 is 17.17 wt.% at 500 °C, followed by a reduction to 12.33 wt.% at 600 °C. Such oil yield reduction is likely due to the increase of gas yield by 10 wt.% at this temperature. Ni/Al_2O_3 has been shown to improve the formation of gaseous hydrocarbons rather than liquid hydrocarbons during catalytic cracking of OPT and PP (Lin et al., 2020; Singh et al., 2019; Xue et al., 2017). This finding is consistent with the lower amount of liquid hydrocarbons obtained at 600 °C, as shown in Fig. 4. On the other hand, the gas yield increases with rising temperatures from 500 to 700 °C for three cases (Fig. 3). The secondary reaction of primary volatiles into lighter compounds at higher temperatures results in the formation of non-condensable gases, increasing gas yield with temperature (Hassan et al., 2019).

3.3. Oil composition analysis

Fig. 4 shows the oil composition obtained from the non-catalytic and catalytic co-pyrolysis of OPT and PP with Ni–Mo/TiO_2 and Ni/Al_2O_3 in the temperature range of 500–700 °C. The oil from non-catalytic co-pyrolysis consists mainly of oxygenated (39.74–52.10%) and phenolic compounds (34.01–41.85%). The oil contains a small amount of hydrocarbons (5.19–10.22%), as evidenced by the relatively low GC-MS relative area for these components. During non-catalytic co-pyrolysis, the oxygenated and phenolic compounds are generated from the thermal decomposition of OPT (i.e., hemicellulose, cellulose, and lignin) (Palamanit et al., 2019; Stefanidis et al., 2014). The thermal degradation of PP produces hydrocarbons *via* a series of reactions that include random chain scission, mid-chain β-scission, end chain β-scission, radical recombination, and hydrogen transfer reactions (Singh et al., 2019; Xue et al., 2017).

When Ni–Mo/TiO_2 and Ni/Al_2O_3 are used as the catalysts in the co-

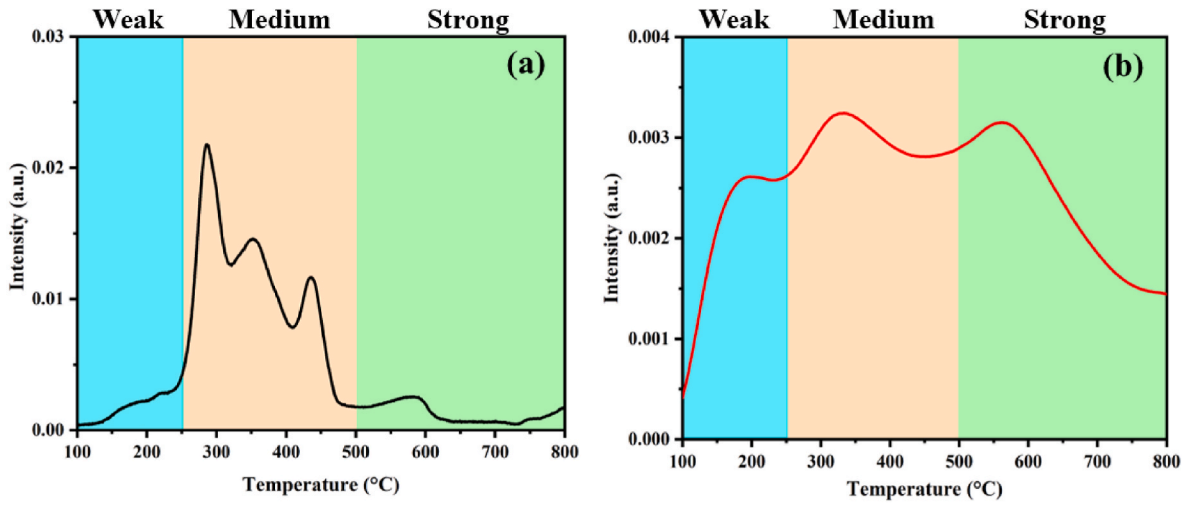

Fig. 1. NH_3-TPD profile of **(a)** Ni–Mo/TiO_2 and **(b)** Ni/Al_2O_3.

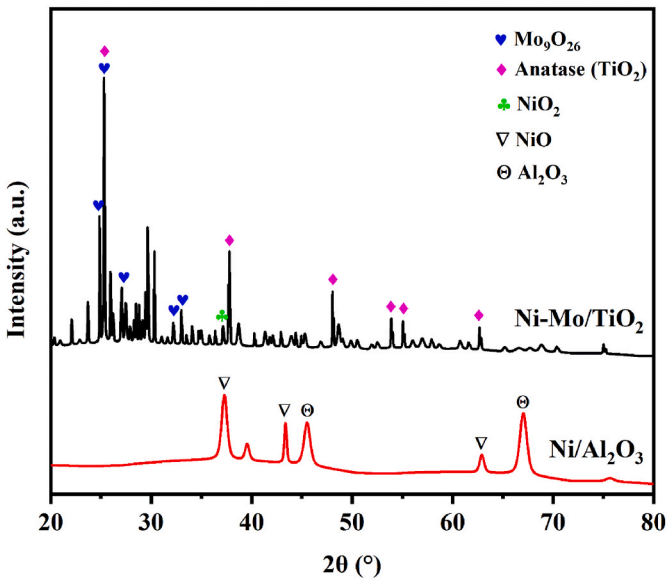

Fig. 2. Powder XRD patterns of Ni–Mo/TiO_2 and Ni/Al_2O_3.

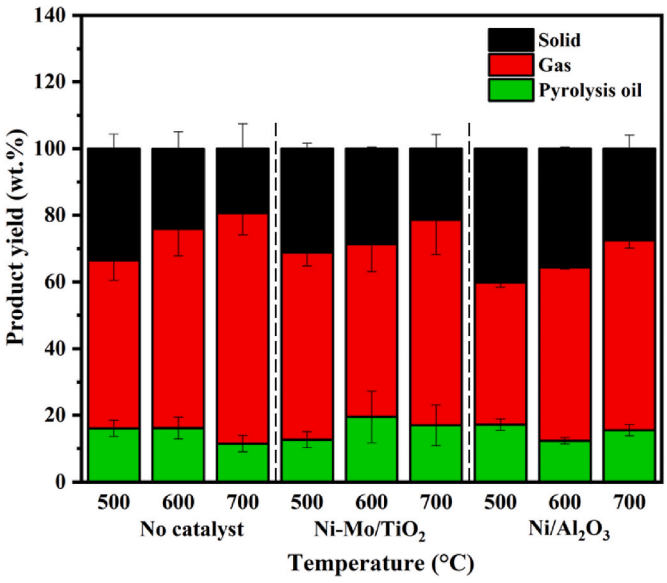

Fig. 3. Product yield from non-catalytic and catalytic co-pyrolysis of OPT and PP with Ni–Mo/TiO_2 and Ni/Al_2O_3 catalysts. Data for non-catalytic co-pyrolysis are from our previous work (Terry et al., 2023). The term "solid yield" refers to the total amount of solid residue collected from the experiments, which includes feedstock residue, catalysts, and coke.

pyrolysis of OPT and PP, the hydrocarbons contained in the oil are significantly increased, as shown by an increase in the GC-MS relative area of up to 54.07–58.18% and 37.28–68.77%, respectively (Fig. 4). The amount of phenolic compounds is reduced, with the reduction in the GC-MS relative area for Ni–Mo/TiO_2 (down to 8.46–20.16%) and Ni/Al_2O_3 (down to 2.93–14.56%). The presence of catalyst generally reduces the amount of oxygenated compounds, although no clear trend can be drawn concerning the parametric effect of temperature and catalyst type. Fig. 5 illustrates the proposed reaction mechanism for the hydrocarbon formation from the analyses based on relevant previous works (Dai et al., 2020; Lin et al., 2020; Singh et al., 2019; Xue et al., 2017). The increase of the hydrocarbon content in the catalytic co-pyrolysis is due to the catalytic cracking of PP and deoxygenation of oxygenated and phenolic compounds promoted by Ni–Mo/TiO_2 and Ni/Al_2O_3 catalyst in addition to the thermal decomposition of PP (Fig. 5).

The two catalysts used here rely on the presence of both metal (Ni and Ni–Mo) and acidic (TiO_2 and Al_2O_3) sites to provide high deoxygenation ability and thus improve hydrocarbon production. The oxygenated and phenolic compounds undergo deoxygenation reactions *via* dehydration, decarbonylation, and decarboxylation to form hydrocarbons (Fig. 5) (Dai et al., 2020). The oxygen in the oil is removed during deoxygenation reactions with water, carbon dioxide, and carbon monoxide released as by-products. The acidic sites in the two catalysts, TiO_2 and Al_2O_3, tend to the occurrence of dehydration reaction over decarbonylation and decarboxylation reactions, resulting in the removal of oxygen from the oil and its subsequent combination with hydrogen to form water as a by-product (Ding et al., 2020). This reaction pathway nonetheless consumes the hydrogen in the oil, which is required to produce hydrocarbon. The presence of metal sites, namely Ni and Ni–Mo, in the two catalysts is expected to partially counteract this pathway, resulting in a more dominant occurrence of decarbonylation and decarboxylation reactions in Ni–Mo/TiO_2 and Ni/Al_2O_3-catalyzed co-pyrolysis of OPT and PP (Balasundram et al., 2018; Dai et al., 2020). Higher acidity of Ni–Mo/TiO_2 relative to Ni/Al_2O_3 (Table 1) due to more abundant acidic sites and synergy between Ni and Mo leads to the formation of a higher amount of hydrocarbons from the catalytic co-pyrolysis of OPT and PP (Fig. 4).

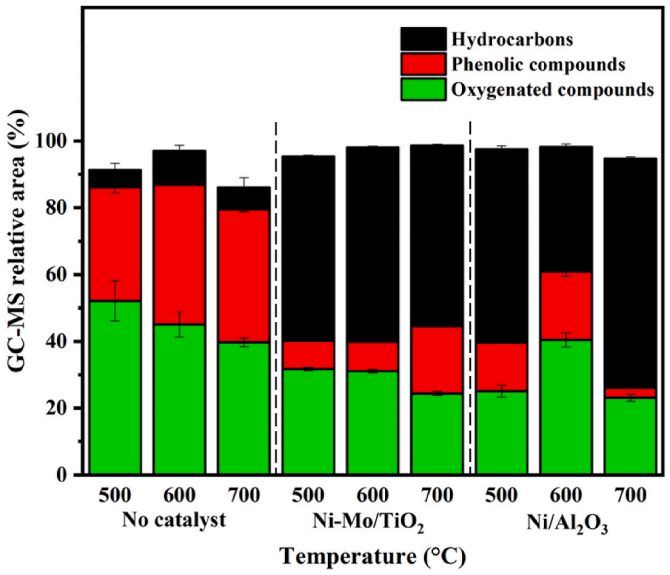

Fig. 4. Oil composition from non-catalytic and catalytic co-pyrolysis of OPT and PP with Ni–Mo/TiO_2 and Ni/Al_2O_3 catalysts. Data for non-catalytic co-pyrolysis is adopted from our previous work (Terry et al., 2023).

During the catalytic co-pyrolysis, the hemicellulose, cellulose, and lignin present in OPT undergo thermal decomposition to produce primary products or intermediates. Afterwards, these products and intermediates diffuse through the pores of Ni–Mo/TiO_2 and Ni/Al_2O_3 and undergo catalytic cracking and deoxygenation reactions to produce secondary products (Balasundram et al., 2018; Lin et al., 2020). The thermal decomposition of hemicellulose primarily yields ketones, furans, and acids, which are then catalytically cracked into smaller oxygenates (i.e., acetic acid, acetone, and simple furans) and olefins on the acidic sites of the catalysts (Dai et al., 2020). Conversely, cellulose is degraded to form anhydrosugars as primary products (Lin et al., 2009). The acidic sites in the two catalysts aid in the dehydration of anhydrosugars to produce more furans. Likewise, the catalytic cracking and deoxygenation of furans form smaller oxygenates and olefins (Dai et al., 2020; Praveen Kumar and Srinivas, 2020). Table 2 shows the decrease of acids and furans in pyrolysis oil after adding Ni–Mo/TiO_2 and Ni/Al_2O_3 catalysts. The result suggests their conversion into olefins, which are the important precursors for the formation of hydrocarbons (Peng et al., 2022). The presence of Ni and Mo in Ni–Mo/TiO_2 promotes the decarbonylation and decarboxylation of oxygenated compounds (i.e., ketones, acids, and furans), producing olefins for the subsequent production of hydrocarbons (Balasundram et al., 2018; Xue et al., 2021). Despite this, the amount of ketones in the oil increases after adding these two catalysts (Table 2). This is likely due to catalyst-promoted radical interactions between OPT and PP (Lin et al., 2020).

Compared to hemicellulose and cellulose, lignin has a more complex structure, thus producing larger molecules of oligomers during thermal decomposition (Jiang et al., 2010; Lu et al., 2010; Stefanidis et al., 2014). The mesoporous structure of Ni–Mo/TiO_2 and Ni/Al_2O_3 catalysts with wide channels allow for higher diffusion of these lignin-derived oligomers, resulting in high conversion into simple phenols (Lu et al., 2010), which are then converted into olefins *via* deoxygenation (Hassan et al., 2019; Xue et al., 2017). During the thermal decomposition of PP, olefins can be produced *via* radical recombination and hydrogen transfer reactions of PP-derived radicals (Singh et al., 2019; Xue et al., 2017). These olefins would produce cyclic hydrocarbons *via* isomerization and oligomerization. The acidic sites in the catalysts have previously been reported to aid in the isomerization and oligomerization reactions resulting in the formation of cyclic hydrocarbons. Fig. 6 shows a higher amount of cyclic hydrocarbons in the oil derived from the catalytic co-pyrolysis than that from the non-catalytic co-pyrolysis (Peng et al., 2022).

Aliphatic hydrocarbons, on the other hand, are produced during PP

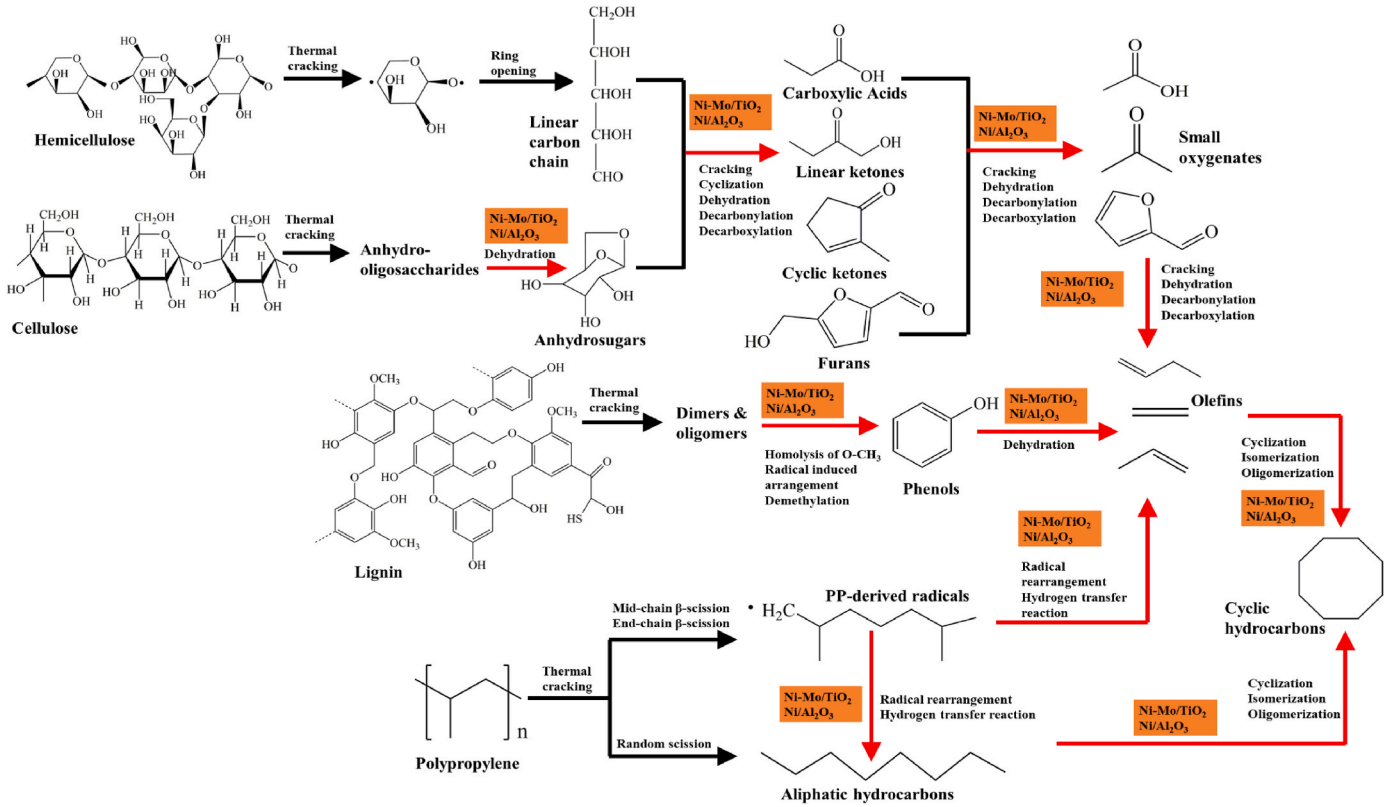

Fig. 5. Proposed reaction mechanism of hydrocarbon formation (Dai et al., 2020; Lin et al., 2020; Singh et al., 2019; Xue et al., 2017).

Table 2
Major oxygenated compounds detected in oil. Data for non-catalytic co-pyrolysis are taken from our previous work (Terry et al., 2023).

Condition	Temperature (°C)	GC-MS relative area (%)		
		Acids	Furans	Ketones
No catalyst	500	7.73 ± 0.93	20.39 ± 1.77	23.67 ± 3.71
	600	7.91 ± 1.07	18.70 ± 2.62	15.81 ± 0.05
	700	13.77 ± 0.60	10.70 ± 0.03	10.38 ± 1.05
Ni–Mo/TiO_2	500	1.20 ± 0.02	0.31 ± 0.03	24.90 ± 0.68
	600	1.82 ± 0.03	–	28.63 ± 0.54
	700	1.26 ± 0.03	0.47 ± 0.00	17.32 ± 0.54
Ni/Al_2O_3	500	2.60 ± 0.04	2.33 ± 0.06	18.84 ± 1.35
	600	1.17 ± 0.04	10.26 ± 0.54	28.42 ± 1.07
	700	–	0.45 ± 0.02	19.06 ± 0.14

decomposition through random chain scission, β-scission, radical recombination, and hydrogen transfer reactions (Singh et al., 2019; Xue et al., 2017). Fig. 6 depicts an increase in aliphatic hydrocarbons in the oil produced by catalytic co-pyrolysis compared to non-catalytic co-pyrolysis. The metal sites (i.e., Ni and Ni–Mo) in the two catalysts promote the hydrogen transfer reactions (Peng et al., 2022). The presence of Mo in Ni–Mo/TiO_2 promotes the transfer of electrons from Mo to Ni, which enhances the catalyst's electron density and thus improves the hydrogen transfer reaction (Maluf and Assaf, 2009). The lower relative amount of aliphatic hydrocarbons observed in Fig. 6 compared to cyclic hydrocarbons is consistent with the nature of aliphatic hydrocarbons as intermediates. Furthermore, some aliphatic hydrocarbons may go through additional isomerization and oligomerization reactions to become cyclic hydrocarbons, facilitated by the acidic sites of the catalysts (Xue et al., 2017). Table 3 compares the catalytic performances of the catalysts used in this work with other works (Imran et al., 2014; Lu et al., 2010; Mysore Prabhakara et al., 2021). Significantly higher content of hydrocarbons is obtained with the use of Ni–Mo/TiO_2 and Ni/Al_2O_3 as compared to the other TiO_2 and Al_2O_3-based catalysts. However, this is also contributed by the addition of PP as the co-feeding material that provides a sufficient hydrogen source. High oxygenated compounds in the oil reported in the other works are expected, mainly from the decomposition of the wood biomass in the presence of TiO_2 and Al_2O_3-based catalysts.

4. Conclusion

Ni–Mo/TiO_2 and Ni/Al_2O_3 are mesoporous acidic catalysts based on nitrogen adsorption-desorption isotherm and NH_3-TPD analyses. Between 500 and 700 °C, the pyrolysis oil yields from the catalytic co-

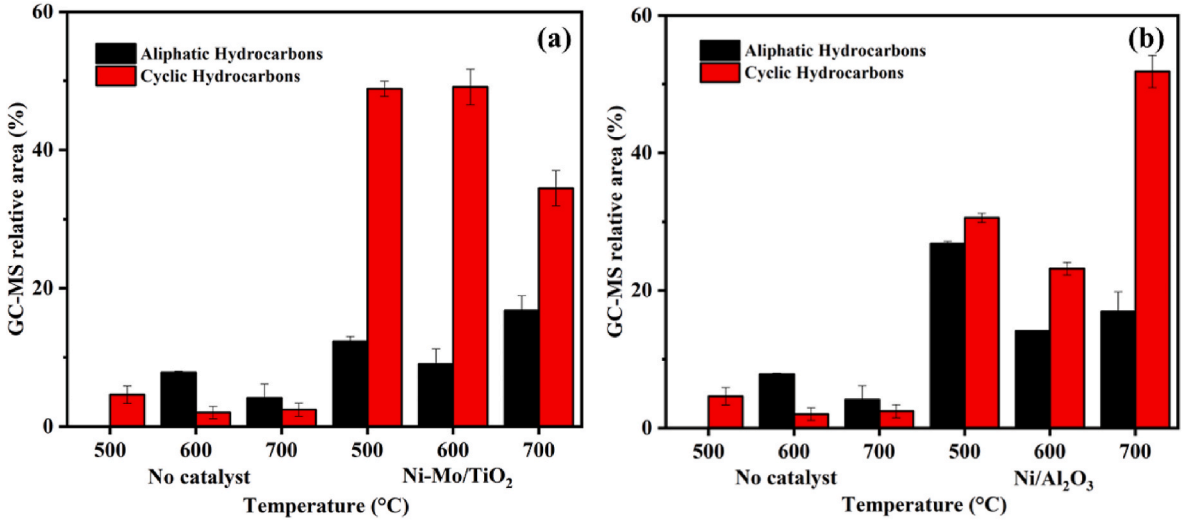

Fig. 6. Types of hydrocarbon detected in oil with **(a)** Ni–Mo/TiO_2 and **(b)** Ni/Al_2O_3.

Table 3
Comparison of the catalytic performances of the catalysts and other relevant works.

Catalyst	Feedstock	Pyrolysis temperature	Hydrocarbons	Oxygenated compounds*	Phenolic compounds	Ref.
		°C	GC-MS relative area%			
Ni–Mo/TiO_2	OPT:PP (1:1)	500, 600 & 700	54.07–58.18	24.4–31.11	8.46–20.16	This work
TiO_2 (Rutile)	Poplar wood	600	0.1	38.3	28	Lu et al. (2010)
Ce/TiO_2 (Rutile)			0.1	39.1	28.8	
Ru–Ce/TiO_2 (Rutile)			0.1	44.1	27.5	
Pd–Ce/Ce/TiO_2 (Rutile)			0.4	37.3	37.2	
TiO_2 (Anatase)			0.1	37.6	28.1	
Ce/TiO_2 (Anatase)			0.3	48.6	17.8	
Ru–Ce/TiO_2 (Anatase)			0.4	49.3	21.3	
Pd–Ce/Ce/TiO_2 (Anatase)			0.7	55.1	18.1	
Ni/Al_2O_3	OPT:PP (1:1)	500, 600 & 700	37.28–68.77	23.1–40.44	2.93–14.56	This work
γ-Al_2O_3	Beechwood	500	7.00	74.00	6.00	Mysore Prabhakara et al. (2021)
Na_2CO_3/γ-Al_2O_3	Wood fibers	500	0.00	30.00	54.00	Imran et al. (2014)

Note: *Oxygenated compounds include acids, ketones, furans, and aldehydes.

pyrolysis of OPT and PP using Ni–Mo/TiO_2 and Ni/Al_2O_3 were 12.67–19.50 wt.% and 12.33–17.17 wt.%, respectively. The acidic properties of both catalysts enhanced the production of hydrocarbon in oil by facilitating the deoxygenation of oxygenated and phenolic compounds and the catalytic cracking of PP. By adding transition metals (Ni and Mo) into the acidic TiO_2 and Al_2O_3-based catalysts, the deoxygenation mechanism was shifted towards decarbonylation and decarboxylation, removing oxygen from oil as carbon dioxide and carbon monoxide gases, which can conserve hydrogen for hydrocarbon formation. Compared to the non-catalytic co-pyrolysis case, the high amount of cyclic hydrocarbons in oil from catalytic co-pyrolysis with Ni–Mo/TiO_2 and Ni/Al_2O_3 catalysts indicates their high catalytic ability in promoting the isomerization and oligomerization reactions of olefins and aliphatic hydrocarbons.

Credit author statement

Liza Melia Terry: Methodology, Validation, Formal analysis, Investigation, Visualization, Writing – original draft. Melvin Xin Jie Wee: Methodology, Resources. Jiuan Jing Chew: Supervision, Resources, Writing – review & editing. Deni Shidqi Khaerudini: Resources, Writing – review & editing. Nono Darsono: Resources, Writing – review & editing. Aqsha Aqsha: Conceptualization, Resources, Funding acquisition, Writing – review & editing. Agus Saptoro: Resources, Writing – review & editing. Jaka Sunarso: Supervision, Resources, Writing – review & editing, Project administration, Funding acquisition.

Declaration of competing interest

The authors declare that they have no known competing financial interests or personal relationships that could have appeared to influence the work reported in this paper.

Data availability

Data will be made available on request.

Acknowledgements

Liza Melia Terry gratefully acknowledges the Tun Taib Scholarship from Sarawak Foundation. The authors acknowledge the facilities, scientific, and technical support from Advanced Characterization Laboratories Serpong, National Research and Innovation Agency through E-Layanan Sains, Badan Riset dan Inovasi Nasional. The authors also acknowledge the facilities for GC-MS analysis and funding support from Curtin University Malaysia through Strategic Research Incentives (SRI).

Appendix A. Supplementary data

Supplementary data to this article can be found online at https://doi.org/10.1016/j.envres.2023.115550.

References

Al-Maari, M.A., Ahmad, M.A., Din, A.T.M., Hassan, H., Alsobaai, A.M., 2021. Co-pyrolysis of oil palm empty fruit bunch and oil palm frond with low-density polyethylene and polypropylene for bio-oil production. Arab. J. Chem. 14, 103282 https://doi.org/10.1016/j.arabjc.2021.103282.

Aqsha, A., Katta, L., Mahinpey, N., 2015. Catalytic hydrodeoxygenation of guaiacol as lignin model component using Ni-Mo/TiO_2 and Ni-V/TiO_2 catalysts. Catal. Lett. 145, 1351–1363. https://doi.org/10.1007/s10562-015-1530-7.

Bagheri, S., Muhd Julkapli, N., Bee Abd Hamid, S., 2014. Titanium dioxide as a catalyst support in heterogeneous catalysis. Sci. World J. 2014, 727496 https://doi.org/10.1155/2014/727496.

Balasundram, V., Zaman, K.K., Ibrahim, N., Kasmani, R.M., Isha, R., Hamid, M.K.A., Hasbullah, H., 2018. Catalytic upgrading of pyrolysis vapours over metal modified HZSM-5 *via* in-situ pyrolysis of sugarcane bagasse: effect of nickel to cerium ratio on HZSM-5. J. Anal. Appl. Pyrolysis 134, 309–325. https://doi.org/10.1016/j.jaap.2018.06.021.

Dai, L., Wang, Y., Liu, Y., He, C., Ruan, R., Yu, Z., Jiang, L., Zeng, Z., Wu, Q., 2020. A review on selective production of value-added chemicals *via* catalytic pyrolysis of lignocellulosic biomass. Sci. Total Environ. 749, 142386 https://doi.org/10.1016/j.scitotenv.2020.142386.

Ding, Y.-L., Wang, H.-Q., Xiang, M., Yu, P., Li, R.-Q., Ke, Q.-P., 2020. The effect of Ni-ZSM-5 catalysts on catalytic pyrolysis and hydro-pyrolysis of biomass. Front. Chem. 8 https://doi.org/10.3389/fchem.2020.00790.

Dong, Z., Yang, H., Chen, P., Liu, Z., Chen, Y., Wang, L., Wang, X., Chen, H., 2019. Lignin characterization and catalytic pyrolysis for phenol-rich oil with TiO_2-based catalysts. Energy Fuels 33, 9934–9941. https://doi.org/10.1021/acs.energyfuels.9b02341.

Fan, L., Chen, P., Zhang, Y., Liu, S., Liu, Y., Wang, Y., Dai, L., Ruan, R., 2017. Fast microwave-assisted catalytic co-pyrolysis of lignin and low-density polyethylene with HZSM-5 and MgO for improved bio-oil yield and quality. Bioresour. Technol. 225, 199–205. https://doi.org/10.1016/j.biortech.2016.11.072.

Hassan, H., Lim, J.K., Hameed, B.H., 2019. Catalytic co-pyrolysis of sugarcane bagasse and waste high-density polyethylene over faujasite-type zeolite. Bioresour. Technol. 284, 406–414. https://doi.org/10.1016/j.biortech.2019.03.137.

Imran, A., Bramer, E.A., Seshan, K., Brem, G., 2014. High quality bio-oil from catalytic flash pyrolysis of lignocellulosic biomass over alumina-supported sodium carbonate. Fuel Process. Technol. 127, 72–79. https://doi.org/10.1016/j.fuproc.2014.06.011.

Jiang, G., Nowakowski, D.J., Bridgwater, A.V., 2010. Effect of the temperature on the composition of lignin pyrolysis products. Energy Fuels 24, 4470–4475. https://doi.org/10.1021/ef100363c.

Keim, W., 2010. Petrochemicals: raw material change from fossil to biomass? Petrol. Chem. 50, 298–304. https://doi.org/10.1134/S0965544110040079.

Kumar, R., Strezov, V., Lovell, E., Kan, T., Weldekidan, H., He, J., Dastjerdi, B., Scott, J., 2019. Bio-oil upgrading with catalytic pyrolysis of biomass using copper/zeolite-nickel/zeolite and copper-nickel/zeolite catalysts. Bioresour. Technol. 279, 404–409. https://doi.org/10.1016/j.biortech.2019.01.067.

Li, C., Zhang, L., Gholizadeh, M., Westernhof, R., Cui, Z., Liu, B., Tang, Y., Jin, X., Xu, Z., Hu, X., 2020. Impact of acidic/basic sites of the catalyst on properties of the coke formed in pyrolysis of guaiacol: a model compound of the phenolics in bio-oil. Energy Fuels 34, 11026–11040. https://doi.org/10.1021/acs.energyfuels.0c01794.

Lin, Yu-Chuan, Cho, J., Tompsett, G.A., Westmoreland, P.R., Huber, G.W., 2009. Kinetics and mechanism of cellulose pyrolysis. J. Phys. Chem. C 113, 20097–20107. https://doi.org/10.1021/jp906702p.

Lin, X., Zhang, Z., Wang, Q., Sun, J., 2020. Interactions between biomass-derived components and polypropylene during wood–plastic composite pyrolysis. Biomass Convers. Biorefin. 3345–3357. https://doi.org/10.1007/s13399-020-00861-4.

Lu, Q., Zhang, Y., Tang, Z., Li, W.-Z., Zhu, X.-F., 2010. Catalytic upgrading of biomass fast pyrolysis vapors with titania and zirconia/titania based catalysts. Fuel 89, 2096–2103. https://doi.org/10.1016/j.fuel.2010.02.030.

Machado, H., Cristino, A.F., Orišková, S., Galhano dos Santos, R., 2022. Bio-oil: the next-generation source of chemicals. Reactions 3, 118–137. https://doi.org/10.3390/reactions3010009.

Maluf, S.S., Assaf, E.M., 2009. Ni catalysts with Mo promoter for methane steam reforming. Fuel 88, 1547–1553. https://doi.org/10.1016/j.fuel.2009.03.025.

Martínez, J.D., Veses, A., Mastral, A.M., Murillo, R., Navarro, M.V., Puy, N., Artigues, A., Bartrolí, J., García, T., 2014. Co-pyrolysis of biomass with waste tyres: upgrading of liquid bio-fuel. Fuel Process. Technol. 119, 263–271. https://doi.org/10.1016/j.fuproc.2013.11.015.

Mysore Prabhakara, H., Bramer, E.A., Brem, G., 2021. Biomass fast pyrolysis vapor upgrading over γ-alumina, hydrotalcite, dolomite and effect of Na_2CO_3 loading: a pyro probe GCMS study. Energies 14, 5397. https://doi.org/10.3390/en14175397.

Ozturk, M., Saba, N., Altay, V., Iqbal, R., Hakeem, K.R., Jawaid, M., Ibrahim, F.H., 2017. Biomass and bioenergy: an overview of the development potential in Turkey and Malaysia. Renew. Sustain. Energy Rev. 79, 1285–1302. https://doi.org/10.1016/j.rser.2017.05.111.

Palamanit, A., Khongphakdi, P., Tirawanichakul, Y., Phusunti, N., 2019. Investigation of yields and qualities of pyrolysis products obtained from oil palm biomass using an agitated bed pyrolysis reactor. Biofuel Res. J. 6, 1065–1079. https://doi.org/10.18331/BRJ2019.6.4.3.

Paranjpe, K.Y., 2017. Alpha, beta and gamma alumina as a catalyst—a review. Pharma Innov. 6, 236–238.

Peng, Y., Wang, Y., Ke, L., Dai, L., Wu, Q., Cobb, K., Zeng, Y., Zou, R., Liu, Y., Ruan, R., 2022. A review on catalytic pyrolysis of plastic wastes to high-value products. Energy Convers. Manag. 254, 115243 https://doi.org/10.1016/j.enconman.2022.115243.

Phan, D.-P., Vo, T.K., Le, V.N., Kim, J., Lee, E.Y., 2020. Spray pyrolysis synthesis of bimetallic NiMo/Al_2O_3–TiO_2 catalyst for hydrodeoxygenation of guaiacol: effects of bimetallic composition and reduction temperature. J. Ind. Eng. Chem. 83, 351–358. https://doi.org/10.1016/j.jiec.2019.12.008.

Praveen Kumar, K., Srinivas, S., 2020. Catalytic co-pyrolysis of biomass and plastics (polypropylene and polystyrene) using spent FCC catalyst. Energy Fuels 34, 460–473. https://doi.org/10.1021/acs.energyfuels.9b03135.

Shafaghat, H., Lee, H.W., Tsang, Y.F., Oh, D., Jae, J., Jung, S.-C., Ko, C.H., Lam, S.S., Park, Y.-K., 2019. In-situ and ex-situ catalytic pyrolysis/co-pyrolysis of empty fruit bunches using mesostructured aluminosilicate catalysts. Chem. Eng. J. 366, 330–338. https://doi.org/10.1016/j.cej.2019.02.055.

Singh, R.K., Ruj, B., Sadhukhan, A.K., Gupta, P., 2019. Thermal degradation of waste plastics under non-sweeping atmosphere: Part 1: effect of temperature, product optimization, and degradation mechanism. J. Environ. Manag. 239, 395–406. https://doi.org/10.1016/j.jenvman.2019.03.067.

Speight, J.G., 2011. Chapter 12 - petrochemicals. In: Speight, J.G. (Ed.), Handbook of Industrial Hydrocarbon Processes. Gulf Professional Publishing, Boston, pp. 429–466.

Stefanidis, S.D., Kalogiannis, K.G., Iliopoulou, E.F., Michailof, C.M., Pilavachi, P.A., Lappas, A.A., 2014. A study of lignocellulosic biomass pyrolysis *via* the pyrolysis of cellulose, hemicellulose and lignin. J. Anal. Appl. Pyrolysis 105, 143–150. https://doi.org/10.1016/j.jaap.2013.10.013.

Terry, L.M., Wee, M.X.J., Chew, J.J., Khaerudini, D.S., Timuda, G.E., Aqsha, A., Saptoro, A., Sunarso, J., 2023. Co-pyrolysis of oil palm trunk and polypropylene: pyrolysis oil composition and formation mechanism. S. Afr. J. Chem. Eng. 43, 348–358. https://doi.org/10.1016/j.sajce.2022.12.001.

Thommes, M., Kaneko, K., Neimark, A.V., Olivier, J.P., Rodriguez-Reinoso, F., Rouquerol, J., Sing, K.S.W., 2015. Physisorption of gases, with special reference to the evaluation of surface area and pore size distribution (IUPAC technical report). Pure Appl. Chem. 87, 1051–1069. https://doi.org/10.1515/pac-2014-1117.

Wang, J., Liu, Q., Zhou, J., Yu, Z., 2020. Production of high-value chemicals by biomass pyrolysis with metal oxides and zeolites. Waste Biomass Valorization 12, 3049–3057. https://doi.org/10.1007/s12649-020-00962-1.

Xue, J., Zhuo, J., Liu, M., Chi, Y., Zhang, D., Yao, Q., 2017. Synergetic effect of co-pyrolysis of cellulose and polypropylene over an all-silica mesoporous catalyst MCM-41 using thermogravimetry–fourier transform infrared spectroscopy and pyrolysis–gas chromatography–mass spectrometry. Energy Fuels 31, 9576–9584. https://doi.org/10.1021/acs.energyfuels.7b01651.

Xue, S., Luo, Z., Zhou, Q., Sun, H., Du, L., 2021. Regulation mechanism of three key parameters on catalytic characterization of molybdenum modified bimetallic micro-mesoporous catalysts during catalytic fast pyrolysis of enzymatic hydrolysis lignin. Bioresour. Technol. 337, 125396 https://doi.org/10.1016/j.biortech.2021.125396.

Zhang, X., Lei, H., Chen, S., Wu, J., 2016. Catalytic co-pyrolysis of lignocellulosic biomass with polymers: a critical review. Green Chem. 18, 4145–4169. https://doi.org/10.1039/C6GC00911E.

Zhou, L., Yang, H., Wu, H., Wang, M., Cheng, D., 2013. Catalytic pyrolysis of rice husk by mixing with zinc oxide: characterization of bio-oil and its rheological behavior. Fuel Process. Technol. 106, 385–391. https://doi.org/10.1016/j.fuproc.2012.09.003.

Zhou, Y., Chen, Z., Gong, H., Chen, L., Yu, H., Wu, W., 2019. Characteristics of dehydration during rice husk pyrolysis and catalytic mechanism of dehydration reaction with $NiO/\gamma\text{-}Al_2O_3$ as catalyst. Fuel 245, 131–138. https://doi.org/10.1016/j.fuel.2019.02.059.